

Seismic fragility curves of single storey RC precast structures by comparing different Italian codes

Dumitru Beilic¹, Chiara Casotto², Roberto Nascimbene^{*1}, Daniele Cicola¹ and Daniela Rodrigues¹

¹EUCENTRE, Pavia, Italy

²ROSE Programme, UME School, IUSS Pavia, Italy

(Received July 31, 2016, Revised February 15, 2017, Accepted February 24, 2017)

Abstract. The seismic events in Northern Italy, May 2012, have revealed the seismic vulnerability of typical Italian precast industrial buildings. The aim of this paper is to present a seismic fragility model for Italian RC precast buildings, to be used in earthquake loss estimation and seismic risk assessment by comparing two building typologies and three different codes: D.M. 3-03-1975, D.M. 16-01-1996 and current Italian building code that has been released in 2008. Based on geometric characteristics and design procedure applied, ten different building classes were identified. A Monte Carlo simulation was performed for each building class in order to generate the building stock used for the development of fragility curves through analytical method. The probabilistic distributions of geometry were mainly obtained from data collected from 650 field surveys, while the material properties were deduced from the code in place at the time of construction or from expert opinion. The structures were modelled in 2D frameworks; since the past seismic events have identified the beam-column connection as the weakest element of precast buildings, two different modelling solutions were adopted to develop fragility curves: a simple model with post processing required to detect connection collapse and an innovative modelling solution able to reproduce the real behaviour of the connection during the analysis. Fragility curves were derived using both nonlinear static and dynamic analysis.

Keywords: seismic fragility; RC precast structures; beam-column connection collapse; nonlinear modelling

1. Introduction

Seismic vulnerability is a measure of how prone a building is to suffer damage for a given intensity of ground shaking, and it can be mathematically formulated by fragility curves. Different methods can be used to develop fragility functions in the earthquake engineering field: empirical curves, based on damage distributions observed in post-earthquake surveys; expert opinion-based curves; analytical curves, obtained through structural analysis of numerical models, and hybrid curves, which can combine any of the previous methodologies in order to compensate for their respective drawbacks (Calvi *et al.* 2006).

Fragility models have been developed mostly for residential buildings, especially cast-in-place reinforced concrete (RC) and masonry structures (Ahmad *et al.* 2011, Karantoni *et al.* 2011, Ozmen *et al.* 2010, Polese *et al.* 2008, Verderame *et al.* 2001), while precast RC structures have been considered only in the last few years (Senel and Kayhan 2010, Babic and Dolsek 2016, Banerjee *et al.* 2016, Casotto *et al.* 2015, Yazgan 2015).

The sequence of seismic events that hit the Emilia-Romagna region (Northern Italy), in May 2012, exposed the high seismic vulnerability of typical Italian precast industrial buildings (Artioli *et al.* 2013, Belleri *et al.* 2014, 2015, Ercolino *et al.* 2016). These events were earthquakes

of low-medium magnitude, yet they had a huge impact in terms of loss of lives, economic losses for business interruptions and damage to the buildings (Marzo *et al.* 2012, Savoia *et al.* 2012). The most common cause of collapse, in industrial buildings, was the inadequacy of the connections of horizontal structural elements (roof panels and beams), to resist the seismic forces or to accommodate the displacement demands. In many cases connections relied only on friction, but in others, even the presence of a mechanical connection (pins or dowels) was unable to arrest the collapse (Clementi *et al.* 2016). The columns of precast structure showed loss of verticality due to a rotation in the foundation element, plastic hinge development at the base, shear failure due to the interaction with traditional masonry infill systems.

Causes of the observed poor seismic behavior are attributed to three main factors: i) Insufficient code provisions and hazard characterization by the time the structures were designed and built, ii) the intrinsic lack of redundancy of the structural system and as mentioned above iii) the design and detailing of beam-to-column connections.

Regarding the first aspect, it is noted that a large number of industrial buildings that exhibited poor seismic behavior, during the mentioned earthquake sequence, were designed before the introduction and enforcement of the more recent Italian building code in 2008 (*Decreto Ministeriale* D.M. 14-01-2008 or NTC2008), and exhibit several structural deficiencies (Belleri *et al.* 2014, Magliulo *et al.* 2014a, b). It is also noted that the first seismic design regulation for this structural system was introduced in Italy only in 1987 (through the D.M. 03-12-1987); yet a seismic hazard

*Corresponding author, Ph.D.

E-mail: roberto.nascimbene@eucentre.it

zonation of the Italian territory that adequately considered the hazard in the Emilia-Romagna region was not released until 2003 (*Ordinanza* n. 3274).

The conventional structural system used in Italian industrial buildings is similar to a portal frame system and consists of tall cantilevered columns, with simply supported beams on top. The lack of redundancy of the system along with its high flexibility render it more vulnerable to seismic excitation when compared against a traditional cast-in-place RC moment frame structure that presents moment-resisting beam-to-column connections and a level of continuity between structural members.

The third factor, the connection between precast beams and columns, represents the critical component that mainly affects the response of a precast structure; its behavior will be deeply investigated in this work, considering different modeling approaches.

2. Aim of the work

The aim of this work is the development of fragility curves for precast structures, considering the structural deficiencies and poor behaviour highlighted by the seismic events in Emilia-Romagna in 2012. To this aim, the procedure presented in Casotto *et al.* (2015), was adopted for the derivation of analytic fragility functions. The procedure is explained with reference to Fig. 1, and consists of three steps: 1) *random generation of precast RC structures*, 2) *design, numerical modelling and damage analyses*, and 3) *fragility curves derivation*.

In order to generate sample structures representative of the Italian building stock, Casotto *et al.* (2015), identified and classified industrial buildings based on two criteria; namely the structural typology and the likely design code used for structural design (as a function of the year of construction). Furthermore, Casotto *et al.* (2015) considered only structures designed before the NTC2008; in this work, even knowing that a limited number of precast buildings have been constructed in recent years, a new category of modern Italian code-conforming industrial buildings was introduced in the structural classification.

As highlighted by Magliulo *et al.* (2012), the seismic response exhibited by precast structures during Emilia earthquake was heavily affected by the connection behaviour; therefore, in this work, two different modelling approaches were compared: the first one consists of a simple pin-connected joint, as presented in Casotto *et al.* (2015); and the second one, in which the connection is modelled with spring elements capable of reproducing the effective contribution of the two resisting mechanisms, dowel action and friction, along with the relative deformations between beam and column, and unseating of the girder (Deyanova *et al.* 2014). Further details on the modelling approach variants are presented in section 6.

3. Classification of italian precast industrial buildings

The classification of the Italian precast industrial building stock, presented in Casotto *et al.* (2015), allowed the characterisation of the common geometric configurations.

This classification was developed using information from different sources such as precast element producers, design reports from Calvi *et al.* (2006, 2009), and from the direct survey of 650 warehouses built between 1960 and 2010 in the Tuscany, Emilia Romagna and Piemonte regions. Part of the surveyed data were provided by the Seismic Risk Prevention Area of the Tuscany Region, that conducted a campaign for risk and hazard assessment in industrial areas (for further information see Ferrini *et al.* 2007). Additional information was collected by the Structural-Analysis Section of the European Centre for Training and Research in Earthquake Engineering (Bellotti *et al.* 2014).

The classification effort resulted in the two structural typologies shown in Table 1. The first typology, more traditional and frequently used, presents a series of independent, one-storey, 2-bay portal frames acting in parallel; with cantilever columns and simply supported beams. The second typology consists of one-storey frames linked by perpendicular beams that carry a main roof beam or that directly support large-span slab elements.

As in Casotto *et al.* (2015), the building stock considered, corresponds to structures constructed within the last 50-60 years. In addition the building stock was divided in three categories in correspondence to the building code

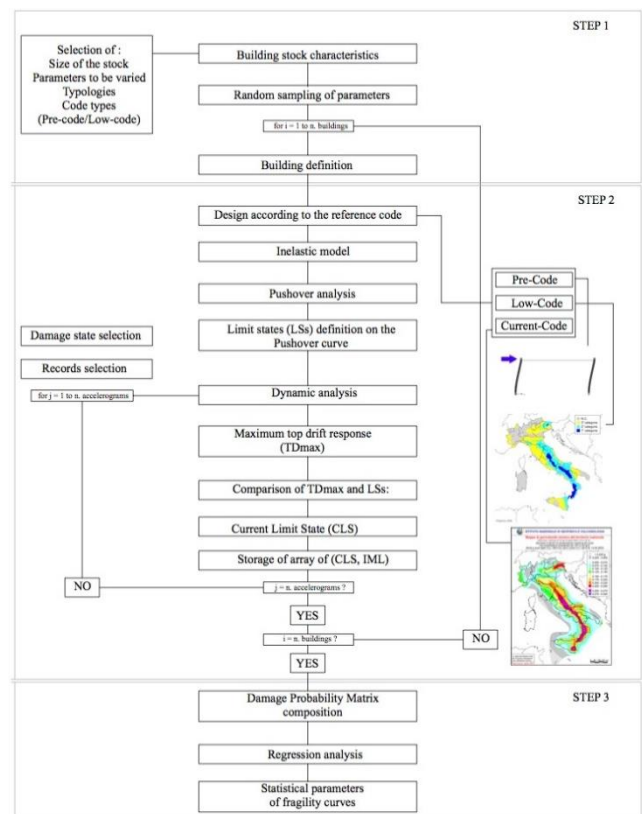


Fig. 1 Flowchart of the proposed analytical method to derive fragility curves [Adapted from Casotto *et al.* 2015]

they should conform to. The first category was defined as *pre-code* and refers to structures designed before the 1996 building code (D.M. 16-01-1996). The second category or *low-code*, corresponds to structures built after the 1996 and before the introduction of the current code of practice, the NTC2008. The last category, was defined as *current-code*, and refers obviously, to structures built after 2008.

The procedure for the estimation of design seismic actions was chosen in agreement with the practices suggested in each building code. Hence, for the current-code category, it was computed from the response spectrum; which was, in turn, defined according to the seismic hazard of the site of construction. For pre-code and low-code designs horizontal loads correspond to a percentage of the seismic weight of the building: 2% for pre-code designs and a variable figure between 4%, 7% and 10% (for seismic zones III, II and I, respectively) for low-code designs, depending on the seismic region where the structure was located.

The resulting low-code and current-code designs were analyzed using the two different modelling solutions adopted for the connections, the simple hinge solution (Casotto *et al.* 2015) and the improved version (Deyanova *et al.* 2014). The pre-code designs were analyzed only for the simple hinge solution.

Table 1 summarises the classification of the building stock according to the structural configuration, reference code, design lateral load and modelling solution for connections. A tag or Id code was assigned to each building class and will be used through the rest of the paper.

4. Generation of precast RC structures

The data collected from the sources previously described were used to derive the statistical distributions of the geometric properties for each building typology. Several distributions were considered; the maximum likelihood method was adopted to select the probabilistic model that provided the best fit (chi-square test) of the data. Table 2 summarises the distributions considered for the geometric properties of the building stock: bay length of the frame L_{beam} , distance between frames $L_{intercol}$ and column height H_{col} . Some information required for this study (e.g., material properties and design loads) could not be extracted from the surveys, and was instead obtained from the literature or from expert opinion. Table 3 reports the loads applied in the simulated design: roof weight G_R , beam weight G_B , lateral beam weight G_{LB} and live load Q .

The concrete and steel characteristic strengths were sampled according to the construction age and the properties indicated by the reference codes (DM 3-03-1975, DM 16-01-1996, DM 14-01-2008). The difference between the actual characteristic strengths of the materials to be used in the modelling and the values indicated in the codes for the design was considered through the results of previous work (Verderame *et al.* 2001), or through overstrength coefficients in the cases where statistical studies were not available.

For pre-code category both smooth and ribbed bars were

considered since the use of ribbed bars increased significantly during the reference period, from 5% in 1950 to 80% in 1980 (Verderame *et al.* 2001).

For pre-code and low-code categories, the tensile strength of the smooth steel bars used in the numerical modelling was taken directly from experimental tests conducted by Verderame *et al.* (2001). The characteristic strengths of ribbed bars and concrete, for numerical modelling, were estimated from the code design values and the overstrength coefficients for steel γ_s (normal distribution with mean value of 1.15 and standard deviation equal to 0.075) and concrete γ_c (normal distribution with mean value of 1.3 and standard deviation equal to 0.15), as suggested in Bolognini *et al.* (2008). Since usually the characteristics of the materials are unknown during the assessment of an existing building, the overstrength coefficients were not applied to the values adopted in the design, but to new

Table 1 Classification of the building classes used in this study

Structural configuration	Code level	Connection	Design lateral load	Id code
 <p>Type 1</p>	Pre-code [Casotto <i>et al.</i>]	Simple [Casotto <i>et al.</i>]	2%	T1-PC-2
		Simple [Casotto <i>et al.</i>]	4%	T1-LC-4
		Improved (This work)	4%	IC- T1-LC-4
	Low-code [Casotto <i>et al.</i>]	Simple [Casotto <i>et al.</i>]	7%	T1-LC-7
		Improved (This work)	7%	IC- T1-LC-7
		Simple [Casotto <i>et al.</i>]	10%	T1-LC-10
		Improved (This work)	10%	IC- T1-LC-10
	Current-code (This work)	Simple [Casotto <i>et al.</i>]	Site construction	T1-CC
		Improved (This work)	Site construction	IC-T1-CC
	 <p>Type 2</p>	Pre-code [Casotto <i>et al.</i>]	Simple [Casotto <i>et al.</i>]	2%
Simple [Casotto <i>et al.</i>]			4%	T2-LC-4
Improved (This work)			4%	IC-T2-LC-4
Low-code [Casotto <i>et al.</i>]		Simple [Casotto <i>et al.</i>]	7%	T2-LC-7
		Improved (This work)	7%	IC-T2-LC-7
		Simple [Casotto <i>et al.</i>]	10%	T2-LC-10
		Improved (This work)	10%	IC-T2-LC-10
Current-code (This work)		Simple [Casotto <i>et al.</i>]	Site construction	T2-CC
		Improved (This work)	Site construction	IC-T2-CC
<i>T1-T2: type of structure</i>		2-4-7-10: % of weight used for the lateral load in PC and LC		
<i>PC-LC-CC: code used for the design</i>		IC: improved connection modelled in this work		

Table 2 Geometric dimensions randomly sampled for the generation of the building stock

Structural configuration	Distribution	m	s	min	max	Source	
Type 1	L _{beam} [m]	Lognormal	2.7	0.3	8	30	Tuscany database
	L _{intercol} [m]	Normal	9	1	8	10	Expert opinion
	H _{col} [m]	Lognormal	1.9	0.2	4	12	Tuscany database
Type 2	L _{beam} [m]	Normal	8.7	2	8	10	Tuscany database
	L _{intercol} [m]	Normal	16.5	3.7	10	25	Tuscany database
	H _{col} [m]	Normal	6.5	1.3	4	11	Tuscany database

Table 3 Load cases randomly sampled

Load Type	Type 1	Type 2	
G _R [kN/m ²]	L _{intercol} < 20 m	2.9	
	L _{intercol} > 20 m	1.6	
GL _B [kN/m]		2.4	
G _B [kN/m]	L _{beam} < 16 m	3.6	4
	16 < L _{beam} < 22 m	5.2	6
	22 < L _{beam} < 24 m	6.85	7.5
	24 < L _{beam} < 28 m	7.5	8
	L _{beam} > 28 m	8.55	9.5
Q [kN/m ²]	normal distribution	μ = 0.5; σ = 0.15; min = 0.0; max = 2	

Table 4 Material properties randomly sampled for the simulated design of the building stock

	Pre-code (all cases)	Low-code (all cases)	Current-code (all cases)
Concrete [MPa]	35, 40, 45, 50	45, 50, 55	45, 50, 55 divided by γ _{co}
Steel [MPa]	320, 380	380, 440	450 divided by γ _{st}

Table 5 Material properties randomly sampled to model the building stock

	Pre-code (all cases)	Low-code (all cases)	Current-code (all cases)
Concrete [MPa]	35, 40, 45, 50 multiplied by γ _c	45, 50, 55 multiplied by γ _c	45, 50, 55
Steel [MPa]	Smooth	Ribbed	Ribbed
	μ = 356 σ = 67.8	380 multiplied by γ _s	380, 440 multiplied by γ _s

randomly sampled values; this allowed to take into account a possible source of uncertainty.

For current-code buildings only steel grade B450C was considered. For concrete, characteristic cube compressive strengths (R_{ck}) were randomly selected between 45, 50 and 55 MPa. Design values were obtained by dividing the characteristic strengths by the partial factor γ_{st} (1.15) for the steel and γ_{co} (1.5) for the concrete.

Table 4 summarises the mechanical properties for

concrete and steel used in the design and Table 5 provides the values used in the numerical modelling.

For each possible combination of structural typology, reference code and design lateral load, 100 structures were generated using a naive Monte Carlo approach. This resulted in a total of 1000 buildings for analysis. These buildings were designed according to the reference code and then subjected to static and dynamic nonlinear analysis to develop fragility curves.

5. Design

The structures were designed in compliance with the pre-code, low-code and current-code classification. The DM 3-03-1975 is the main reference for the pre-code typologies, the DM 16-01-1996 for the low-code, while DM 14-01-2008 is the current-code.

5.1 Code design

Structural design of buildings in the pre-code and low-code categories was carried out using the allowable tension method. Buildings in the current-code category were designed using the limit state design in accordance with NTC2008. A verification of maximum drifts was carried out for the low-code and current-code designs at the end of the design stage. Specific aspects of the structural design are discussed next.

5.1.1 Pre-code and Low-code design

For pre-code and low-code designs the seismic action was applied as a static horizontal force computed as a percentage of the seismic weight of the building.

The value of the seismic load was defined considering several additional aspects: the type of foundation, the structural system and the fundamental period of vibration, evaluated assuming a column size of 50 cm (the minimum column dimension for precast sections). The axial load computed through seismic load combination was increased by the contribution of the vertical acceleration according to the number of bays and the percentage of the seismic weight.

In the low-code design the second order effects were considered amplifying axial and shear load, using factors defined as a function of column slenderness.

Pre-dimensioning of the structural elements was carried out using a modulus of elasticity reduced by 60% to account for cracking. Pre-dimensioning of structural members was accomplished based on three criteria. First, a minimum column size was defined based on elastic buckling considerations (Euler critical axial load). Second, compression stress in concrete was verified under combined moment and axial load, considering small eccentricity. Finally, the shear stress demand was compared with the allowable shear stress. The column size for detailed design was chosen as the smallest section that simultaneously satisfied the above criteria, but not less than 50 cm.

The detailed column design was carried out using a simplified method (r-t method) that accounts for axial-moment interaction, and which allows to define the required

steel area and section depth from the material properties only. The method is summarised in the following equations

$$x = kd \quad (1)$$

$$k = \frac{n\sigma_c}{n\sigma_c + \sigma_s} \quad (2)$$

$$r = r' \sqrt{\frac{1}{\sigma_c \frac{k}{2} \left(1 - \frac{k}{3} + \frac{1 - \delta}{\mu} \left(\frac{1 - k}{k - \delta} - 1 \right) \right)}} \quad (3)$$

$$t = \frac{k^2 r}{2nt'(1 - k - \mu(k - \delta))} \quad (4)$$

$$d = r \sqrt{\frac{M_{ed}}{b}} \quad (5)$$

$$A_s = t \sqrt{M_{ed} b} \quad (6)$$

Where x is the neutral axis depth, d is the effective depth, n is the Modular ratio, assumed equal to 10 for pre-code and 15 for low-code, σ_c e σ_s are the allowable stresses for concrete and steel, r' and t' are defined according to material properties, δ is the concrete cover (3 cm), μ was assumed equal to 1, M_{ed} is the external moment, b is the section width and A_s is the amount of reinforcement required. According to the provisions of D.M. 14-02-1992 the percentage of reinforcement must be between 0.3% and 6% of the gross section area.

The stresses were calculated according to the response state of the section and then compared with the allowable tensions: in case of small eccentricity superposition principle was used, whilst the position of the neutral axis was computed in case of large eccentricity.

The displacement limit was verified only for the low-code design, as specified in the D.M. 16-01-1996. Fig. 2 summarizes the design procedure of pre and low-code, the dashed boxes point out those steps required only by low-code design.

5.1.2 Current-code design

In compliance with the NTC2008, buildings in the current-code category were designed to satisfy the performance criteria of the life safety (SLV) and damage control (SLD) limit states. The performance criteria for the SLV establishes that under the seismic actions corresponding to 475-year return-period event no global or local collapse of the structure shall occur. Furthermore, for SLD limit state, the building or its contents shall not experience damage or operative disruption when subject to a seismic event with return period of 50 years.

Seismic actions were characterized through an elastic acceleration response spectrum, defined, in turn, from the parameters: soil type, peak ground acceleration (a_g), dynamic amplification factor (F_0) and period defining the

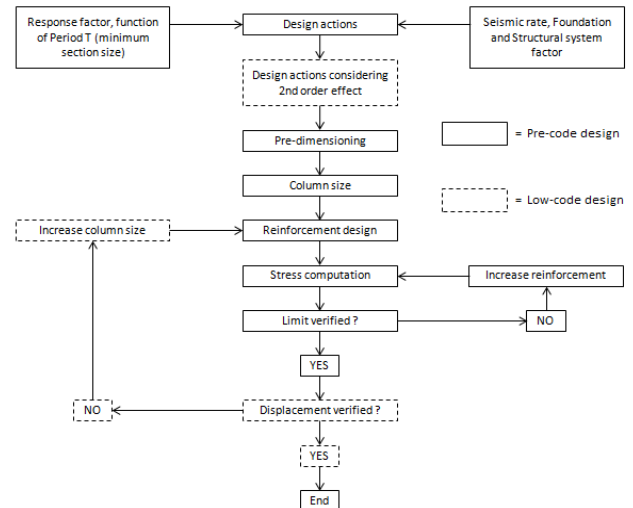


Fig. 2 Pre and low-code design procedure

beginning of the constant velocity response range (T_c^*). A soil type C was adopted in the current study and the corresponding response spectrum parameters for the two hazard levels are: $a_g=0.217g$, $F_0=2.338$ and $T_c^*=0.303s$ for the 475-year return period event; $a_g=0.088g$, $F_0=2.393$ and $T_c^*=0.268s$ for the 50-year event.

The design seismic action for the SLV limit state was obtained reducing the elastic acceleration response spectrum by a behaviour factor (q) of 3.3, that corresponds to one-storey frame structures with low ductility (CDB) according to NTC2008. The three spectra are shown in Fig. 3.

As a starting point on the design process, the size of the columns was set equal to the lower limit for precast sections (50 cm). This allowed the computation of the period of vibration of the structure, and the estimation of the spectral acceleration and seismic force for structural design. The period of vibration was determined using a modulus of elasticity E reduced by 50% to account for cracking.

The pre-dimensioning was performed through the evaluation of second order effects (P-delta) and the displacement verification for SLD limit state. The P-delta effects were evaluated with the simplified method described in the current-code: if θ , the ratio between the second and first order moments, was higher than 10%, the size of the column was increased by 5 cm and the computation of θ iteratively repeated until it was smaller than 10% or the column depth was larger or equal to 1/10 of its height. If, at the end of this iterative procedure, the ratio θ was still higher than 10%, but lower than 20%, the second order effect was addressed just increasing the design actions by a factor equal to $1/(1 - \theta)$. If the ratio was bigger than 20% the size of the columns was further increased and the procedure repeated until the fulfilment of the requirement.

Additionally, a displacement verification was also carried out for the SLD limit state: the maximum displacement shall not exceed 1% of the storey height.

The amount of reinforcement in the column was defined through the construction of the axial load-moment interaction diagram. The provisions of NTC2008 regarding

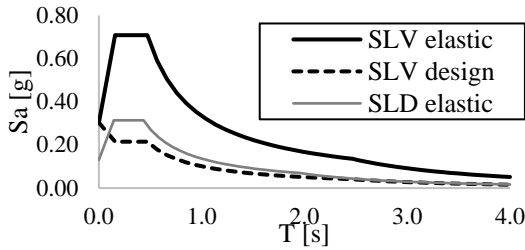


Fig. 3 Acceleration response spectra: Life safety Limit state (SLV) elastic and design spectra, Damage control Limit state (SLD) elastic spectrum

maximum axial load ratios and the amount and spacing of longitudinal reinforcement for columns were met. The current-code design procedure is summarized in Fig. 4.

5.2 Connection design

The type of connection considered in this study consists of a beam sitting on top of a column. For the structures in the pre-code category, the horizontal force transfer between beams and columns relies only on friction. On the other hand, after the introduction of the 1987 building code (D.M. 03-12-1987) the use of steel bolts or bars, for shear transfer, became mandatory. Consequently, connections of structures assigned to the low-code and current-code categories were designed for the combined effect of friction and dowel action. Friction resistance was estimated from beam reactions and the friction shear coefficient of the connection, which depends on the type of contact surfaces between beam and column (concrete, rubber pads or steel plates). The definition of the friction coefficient is a controversial matter, since some literature sources report values between 0.6 and 0.9; whilst, values obtained in experimental campaigns range between 0.1 and 0.5 (Magliulo *et al.* 2011). Due to this uncertainty and to estimate the effect of this parameter on the final fragility curves, a decision was made to adopt two fixed values of 0.2 and 0.3 for the derivation of fragility curves using the first modelling approach (Casotto *et al.* 2015). The first value (0.2) was intended as a lower bound, and the value of 0.3 corresponds to the mean of the range found in Magliulo *et al.* (2011). For the second approach only the more conservative value of 0.2 was considered. For the connection design, beam reactions were reduced by 40% to account for the reduction of gravity forces due to vertical accelerations (Bolognini *et al.* 2008).

The design of the connection consists in the definition of an adequate number and size of steel bars so that the shear resistance associated with steel failure is higher than the shear demand. For low-code designs, the dowel mechanism was designed for the shear force acting on the column, reduced by the friction resistance; while for current code designs, connections were to be designed following capacity design principles; hence, the design shear force was amplified by an overstrength factor γ_{Rd} of 1.

The shear demand was computed as follows

$$V_{ed} = \gamma_{Rd} \frac{M_{Rd}}{H_{col}} \tag{7}$$

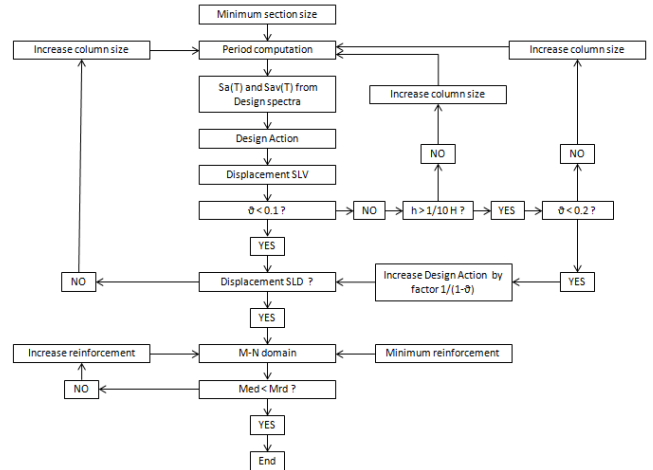


Fig. 4 Current-code design procedure

Where M_{Rd} is the moment capacity of the column and H_{col} is the column height.

Additional details about the design of connections for the low-code and current-code categories can be found in EOTA 2001, and EOTA 2013, respectively.

The resistance of the connection was estimated as the sum of the friction resistance and the dowel capacity; with the latter defined as the smallest shear resistance associated with the three possible failure modes: steel failure, concrete pry-out failure and concrete edge failure.

5.3 Design summary

Relevant design criteria used in the pre-code, low-code and current-code designs are summarized in Table 6.

Table 7 presents the results of the design process. For each class of the building stock, the table reports average values of the following parameters: column size and area, geometric ratio of reinforcement ρ , diameter ϕ of the steel

Table 6 Summary of pre-code, low-code and current-code design methods

	Pre-code	Low-code	Current-code
Seismic action	Static analysis	Static analysis	Static analysis
	Horizontal force 2% of the total weight	Horizontal force: 4%, 7%, 10% of total weight P-Delta effects considered	Horizontal force from design spectra P-Delta effects considered
Design method	Admissible tension	Admissible tension	Limit state
	Flexure and compression for small or big eccentricity	Flexure and compression for small or big eccentricity	Design of longitudinal reinforcement
	Standard shear reinforcement	Design of the shear reinforcement displacements verification	Design of the shear reinforcement (cap. design) displacements verification
Connections	Friction connection	Connections with standard steel elements	Connections with standard steel elements (cap. design)

Table 7 Summary of pre-code, low-code and current-code design results

	Column side [m]	Section area [m ²]	Reinforcement ρ [%]	Dowel diameter ϕ [mm]	Connection shear resistance [kN]
T1-PC-2	0.5	0.25	1.62	-	-
T1-LC-4	0.51	0.26	1.25	12	17.2
T1-LC-7	0.57	0.32	1.45	12	19.8
T1-LC-10	0.61	0.38	1.57	12	22.0
T1-CC	0.69	0.48	1.42	22.7	42.3
T2-PC-2	0.5	0.25	1.60	-	-
T2-LC-4	0.51	0.26	1.32	12	16.9
T2-LC-7	0.57	0.33	1.43	12	19.9
T2-LC-10	0.62	0.39	1.54	12	22.6
T2-CC	0.67	0.46	1.47	24.6	41.9

T1-T2: type of structure *2-4-7-10: % of weight used for the lateral load in PC and LC*
PC-LC-CC: code used for the design

dowel and shear resistance of the connection without considering the friction contribution. Conversely, no evident trend for the variations in reinforcement ratios is observed; this probably because of the change in section dimensions.

In Table 7, shear resistance of the connections is compared in terms of dowel-action resistance only. This in order to highlight the effect of the different design procedures. Since the friction resistance was considered only in the connection design of low-code, the steel dowel required is smaller if compared with the current-code. The difference in the shear resistance presented in the table is due to the seismic provisions adopted for the current code and to the increased size of the column.

6. Numerical modelling and nonlinear analysis

6.1 Modelling approach

As stated in the introduction, the poor response of precast industrial buildings during the 2012 Emilia earthquake, was mainly due to deficiencies in the beam-column connection. In this work two different approaches were considered to model the structure in order to deeply investigate the connection behaviour.

6.1.1 First Modelling Approach

In the first modelling solution, presented in Casotto et al. 2015, the randomly generated structures were modelled in a 2D environment using the software Opensees

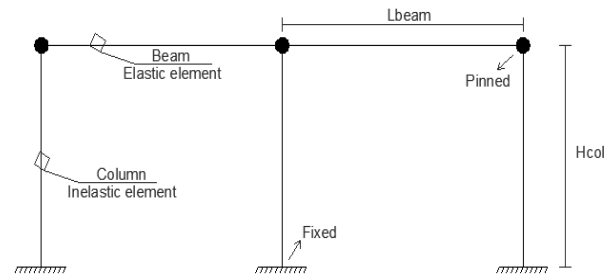


Fig. 5 First modelling approach, 2d Opensees model

(McKenna and Fenves 2010); the structures were analyzed as a single 2D bare-frame. The analyses accounted for p-delta effects and material nonlinearities. Fig. 5 shows the model and some of the assumptions made.

The analysis as a bare-framed system finds justification in the work by Brunesi et al. (2015), who proved that the presence of infill panels is relevant only during the elastic response phase, and that the stiffness of the panel-to-column connections does not inhibit the cantilever-like response of the system. As stated before, the focus of this work is on global failure mechanisms; infill collapse and local damages associated to panels-to-structure connections will be investigated in a further study. It is worth to note that, although the results obtained in Casotto et al. (2015) seem to indicate higher fragilities when a 3D modelling approach is implemented, a 2D model will suffice for the reproduction of the seismic response and the main structural deficiencies.

Column elements were modelled as inelastic force-based fibre elements, with a mesh of 220 fibres and 4 integrations points. The concrete nonlinear behaviour was modelled using the Kent-Park model, modified by Scott et al. (1982). The steel behaviour was simulated using the Menegotto and Pinto 1973 model. The level of prestress in the beams considerably reduces the damage; therefore the assumptions of uncracked sections and elastic behaviour seem to be justified and sufficiently reliable.

A pinned-joint was assigned to the beam-to-column connection, this implied that, identification of the collapse modes associated to connection failure and beam unseating were obtained after post-processing of the analysis results (Casotto et al. 2015). Connection failure was deemed to occur when the recorded shear demands exceeded the connection capacity in at least one column. The condition for beam unseating was reached when the sliding displacement of the beam exceeded its support length d_u , estimated with the following expression

$$d_u = \frac{2}{3} \cdot 0.5 \cdot b \quad (9)$$

Where b is the column depth and the ratio $2/3$ is due to the triangular stress distribution in the contact area between beam and top of the column; this value is then halved in order to account for the worst scenario where the columns oscillate out of phase.

6.1.2 Second modelling approach

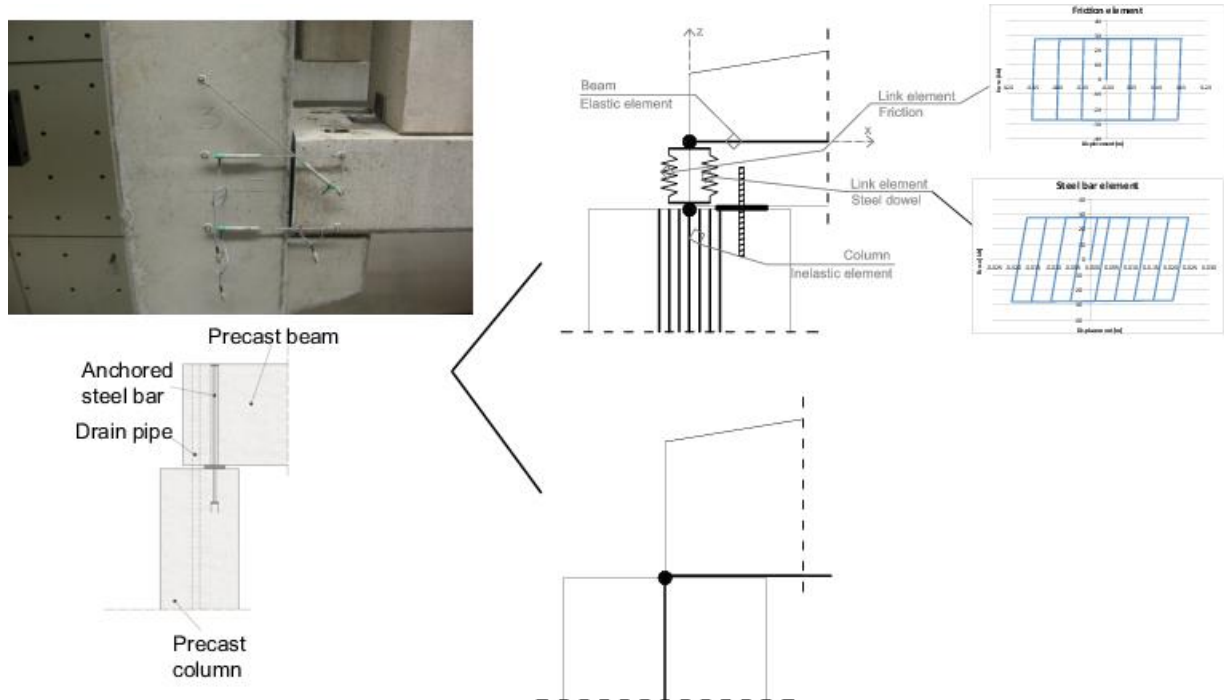


Fig. 6 Modelling solutions for the connection, improved (top) and Casotto *et al.* (2015) (bottom)

Structures assigned to the low-code and current-code categories were also analyzed using a second approach for the connection modelling. Analysis models were developed in the program SeismoStruct (Seismosoft 2016); and as for the previous approach, both geometric and material nonlinearities were considered. The numerical elements used for columns (including number of fibres and integration points) and beams are as described in the first modelling approach. The constitutive laws for the representation of material nonlinearities are the Mander model (Mander *et al.* 1988) for concrete and the bi-linear hysteresis model for reinforcing steel.

The innovation of the second approach is associated with the way the connections were modelled and analyzed: two shear springs, acting in parallel, explicitly reproduced the effective contribution of the friction and dowel-action mechanisms along with the relative displacements between beam and top of the column, and the collapse modes associated to connection failure and unseating of the beams. Fig. 6 shows a schematic of the two modelling approaches.

In the last few years, several researchers (Psycharis and Mouzakis 2012, Toniolo 2012, Magliulo *et al.* 2014, Zoubek *et al.* 2015) have studied the behaviour of beam-column dowel connection. Babic and Dolsek (2016) developed fragility curves for precast building using spring elements. Connections characterized by steel bars were modelled by link elements with a tri-linear force-displacement relation (from Zoubek *et al.* 2014 results). On the other hand, connections relying only on friction were modelled using a spring with an elastic perfectly plastic relationship, where the strength was the product of axial force and friction coefficient.

In this work, a force displacement relationship was defined for each contribution, since only low and current

code were analyzed with the second approach, two separate link elements were modelled for the connections of all buildings, one representing the friction resistance and the other associated to the dowel action.

The force-displacement curve of the spring representing the shear friction mechanism, was defined as follows: i) the initial stiffness branch corresponds to the shear stiffness of the elastomeric pad, and extends until the friction resistance of the connection is reached, and ii) a perfectly-plastic branch with an ultimate displacement corresponding to the beam unseating (Dejanova *et al.* 2014). The ultimate displacement was computed as the support length d_u of the first modelling approach as shown before. Friction resistance of the connection was computed as described in section 5.2.

The monotonic response of the spring representing the dowel mechanism was defined through a bilinear force-displacement curve that consists of an elastic branch and yield plateau with limited ductility. The maximum resistance was assumed as the smallest shear resistance obtained from the three possible failure mechanisms (steel failure, concrete pry-out failure and concrete edge failure) as described in section 5.2. Following the results of Aguiar *et al.* (2012), the yield displacement was set to 0.26ϕ , where ϕ is the diameter of the dowel. From the work of Psycharis and Mouzakis (2012), the ultimate displacement was defined as 3 cm.

The individual force-deformation curves assigned to friction and dowel mechanisms are presented in Fig. 7. The combined response that represents the connection capacity for buildings in the low-code and current-code categories was included for completeness. To account for the possible unseating of beams in the analysis model, zero residual strength was assigned to the force deformation curves. As

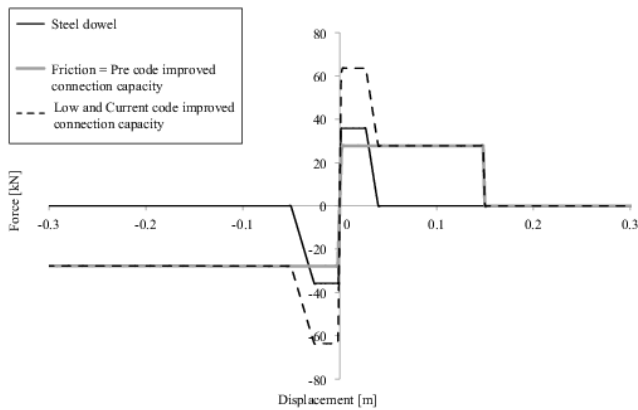


Fig. 7 Force-displacement behaviour for friction and steel link elements

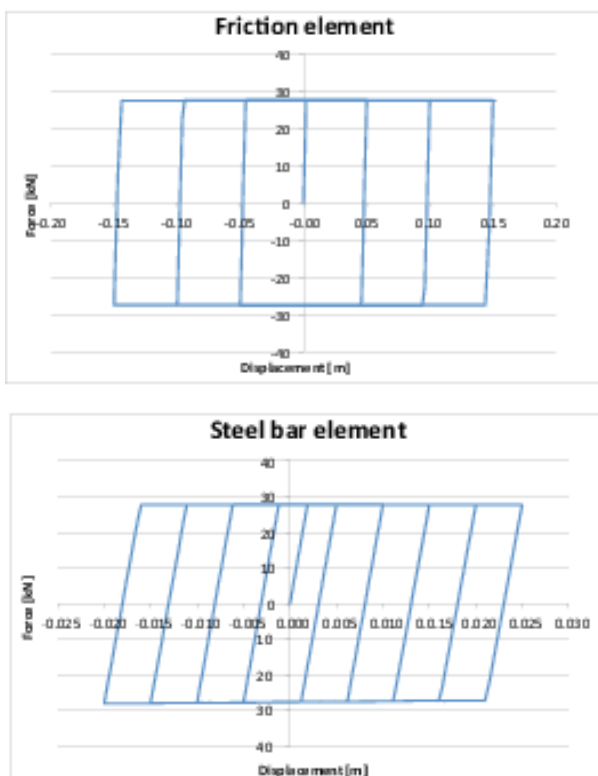


Fig. 8 Force-displacement cyclic behaviour for friction and steel link elements

shown in Fig. 8, an elastic-perfectly plastic hysteresis model was adopted for the cyclic response of the two shear springs. The hysteresis model adopted does not account for stiffness or strength degradation.

6.2 Pushover analysis and damage state definition

A pushover analysis was carried out over each generated building to establish the limit states, and damage levels (or damage states) used in the derivation of fragility curves. Two limit states (LS1 and LS2) and three damage levels (none/slight damage, moderate/extensive damage and collapse), were considered in this study. As suggested in

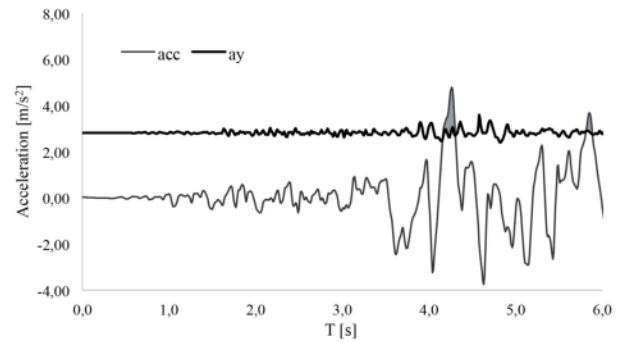


Fig. 9 Newmark sliding block analysis for the evaluation of sliding displacement

Casotto *et al.* (2015), the first limit state (LS1) was attained at yielding of the column longitudinal reinforcement. For the reasons explained also in Casotto *et al.* (2015) and in Brunesi *et al.* (2015), the LS2 or collapse limit state shall not be defined from material strains; instead, this limit was defined as the minimum between a drift limit of 3%, or the displacement/drift corresponding to a 20% drop in capacity in the pushover curve.

The limit state of column shear failure was not considered in this work because it has not been observed in any of the precast industrial structures investigated after the Emilia-Romagna events (Deyanova *et al.* 2014). The flexural collapse was predominant because of the large column sections, designed for buckling, and the slenderness of the column, due to the large inter-storey height.

The collapse limit state was also related to the loss of support of the beam. The assessment of this collapse mode varied depending on the modelling approach considered.

For the first approach, identification of a collapse case involved the estimation of the beam displacements relative to the column (sliding displacement) and the subsequent comparison against the available support length, d_u . As described in Casotto *et al.* (2015), sliding displacements were estimated, with the Newmark's sliding block analysis method (adapted from Kramer 1996), as the double integral of the acceleration at the connection node exceeding the yield acceleration benchmark a_y (shaded area shown in Fig. 9). The yield acceleration time-history was computed as the ratio of the connection shear capacity to the inertial mass tributary to the connection. Variation of the yield acceleration with time, as implied in Fig. 9, is the result of variations in beam reactions.

In the second modelling approach investigated in this work, unseating of beams was a simulated collapse mode; and therefore, no additional post-processing operation was required.

6.3 Dynamic analyses and seismic input

To the previously described structural model the following additions were made for the dynamic analyses: the masses were lumped at the beam-column joint and a tangent stiffness proportional damping model was used with a damping ratio of 2% (McKenna *et al.* 2010). The structure

was subjected to unidirectional, horizontal and vertical ground acceleration.

A total of seventy records were extracted from the PEER database, with magnitudes ranging between 4 and 6.5 and distances from 0 to 30 km, as indicated by the disaggregation analysis, in Northern-Central Italy for the 2475 years return period hazard and for S_a ($T=1.5$ s), (Iervolino *et al.* 2011). A low scaling factor of approximately 1.5 (an acceptable factor according to Watson-Lamprey and Abrahamson 2006) was applied to 13 of the ground motion records in order to simulate stronger earthquake intensities.

7. Fragility curve derivation

For each structure and ground motion the maximum response, expressed in terms of maximum top displacement, was recorded and then, compared against the limit states defined from the pushover analyses to allocate each analysis into a damage level. All the frames within a given damage state were summed up and normalized with respect to the total number of buildings to compute the Damage Probability Matrix (DPM). This matrix contains the percentage of frames in each damage state for a set of intensity measure levels representing each ground motion record.

Then the cumulative fractions of structures in each damage state for each intensity level, expressing the probability of exceeding the damage state, were estimated and fitted with a lognormal cumulative distribution function. The regression analysis was carried out using the maximum likelihood method.

In Casotto *et al.* (2015) various intensity measures were considered and compared in the fragility curve derivation. The R^2 coefficient was used as a measure of the correlation between the intensity levels and the cumulative percentage of frames within a given damage state. The use of peak ground acceleration (PGA) led to a very large dispersion in the results, whilst a considerably increased correlation with damage was found using Spectral acceleration (S_a). The period of vibration for which the S_a is computed and its influence on the variability of the fragility curves was thus investigated in the correlation analysis shown in Fig. 10, where the coefficient R^2 is computed for a set of elastic periods (Silva *et al.* 2015). The mean R^2 curve (the mean between the first limit state and the second limit state R^2 curves) is also presented and the optimal period (the period corresponding to the maximum correlation for the mean R^2 curve) is indicated with a vertical line. It is evident that the selection of the period may lead to values of coefficient R^2 far from 1, resulting in a very low efficiency of the intensity measure (as showed for PGA in Casotto *et al.* 2015). The spectral acceleration at the mean optimal period of vibration $S_a(T_{opt})$ was selected to be used as the intensity measure, because it almost coincides with the optimal period of the second limit state curve (which provides information about the damage with more influence on losses) without substantially compromising the first limit state correlation.

This correlation analysis was repeated for all the classes

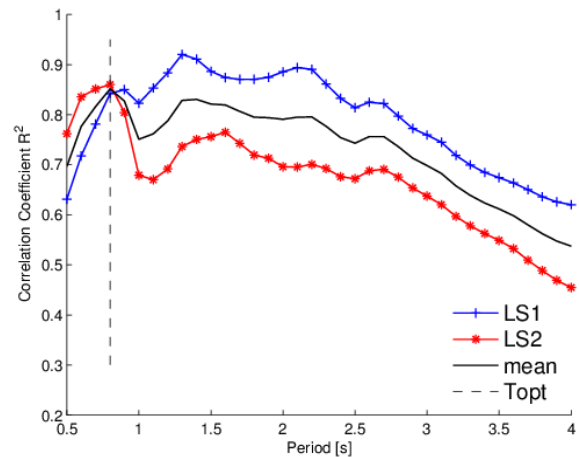


Fig. 10 Correlation coefficient as a function of the period of vibration of S_a , for T1-PC-2 model

of the building stock, leading to different optimal periods for each of them; obviously the optimal period would change if any other function, rather than the lognormal cumulative distribution function was used.

8. Results and discussions

The final fragility curves derived with the two approaches previously discussed are presented in this section. Most of the fragility functions obtained with the first modelling approach are presented in Casotto *et al.* (2015); in this work only the results obtained for the low-code designs (with second modelling approach) and current-code designs (with both modelling approaches) will be presented.

8.1 First modelling approach

The parameters for yield and collapse fragility curves (LS1 and LS2, respectively) of all building classes, analyzed with the first modelling approach, are reported in Table 8. From this table it can be noted that, for a given code category, there are no relevant differences between the model parameters (θ and σ) of the two structural typologies (T1 and T2); whilst significant differences are observed between buildings designed with different codes. It is clear from the comparison between fragility curve parameters shown in Table 8 that for current-code structures the probability of collapse is significantly reduced due to the efficiency of the limit state design.

It should be noted that a direct comparison between the fragility curves derived for different building classes is not appropriate, given that they were derived for different optimal periods (T_{opt}); hence they will be presented in different plots. These fragility functions would need to be applied within a complete loss assessment exercise in order to fully appreciate the differences between them.

Fig. 11 (left) presents a comparison between collapse fragility curves evaluated considering only flexural failure of the column and the combined fragility of both,

Table 8 Results from the first approach. Median (θ) and logarithmic standard deviation (σ), and coefficient of correlation (R^2) of each fragility function using an intensity measure of $S_a(T_{opt})$ in g

Id code	Friction coefficient = 0.2								Friction coefficient = 0.3					
	LS1				LS2				LS1				LS2	
	T_{opt}	θ	σ	R_{LS1}^2	θ	σ	R_{LS2}^2	T_{opt}	θ	σ	R_{LS1}^2	θ	σ	R_{LS2}^2
T1-PC-2	0.8	0.21	0.59	0.84	0.36	0.59	0.86	1.6	0.09	0.56	0.89	0.29	0.52	0.76
T1-LC-4	1.8	0.09	0.49	0.91	0.26	0.40	0.88	1.8	0.09	0.49	0.91	0.27	0.30	0.89
T1-LC-7	0.8	0.27	0.48	0.89	0.60	0.50	0.77	1.3	0.16	0.48	0.90	0.59	0.51	0.66
T1-LC-10	0.8	0.31	0.38	0.92	0.39	0.47	0.87	0.8	0.33	0.39	0.92	0.74	0.61	0.69
T1-CC	0.7	0.34	0.36	0.91	1.03	0.66	0.66	0.9	0.27	0.33	0.87	1.27	0.55	0.72
T2-PC-2	1.7	0.07	0.55	0.89	0.16	0.61	0.73	1.7	0.08	0.54	0.90	0.27	0.42	0.85
T2-LC-4	1.8	0.08	0.47	0.91	0.24	0.38	0.88	1.8	0.08	0.47	0.91	0.25	0.28	0.90
T2-LC-7	0.8	0.24	0.44	0.88	0.58	0.46	0.76	1.3	0.14	0.45	0.91	0.51	0.38	0.74
T2-LC-10	0.8	0.29	0.39	0.93	0.46	0.53	0.81	0.8	0.30	0.40	0.93	0.85	0.61	0.62
T2-CC	0.7	0.34	0.34	0.92	0.98	0.65	0.63	0.9	0.27	0.32	0.87	1.33	0.60	0.63

T1-T2: type of structure

2-4-7-10: % of weight used for the lateral load in PC and LC

PC-LC-CC: code used for the design

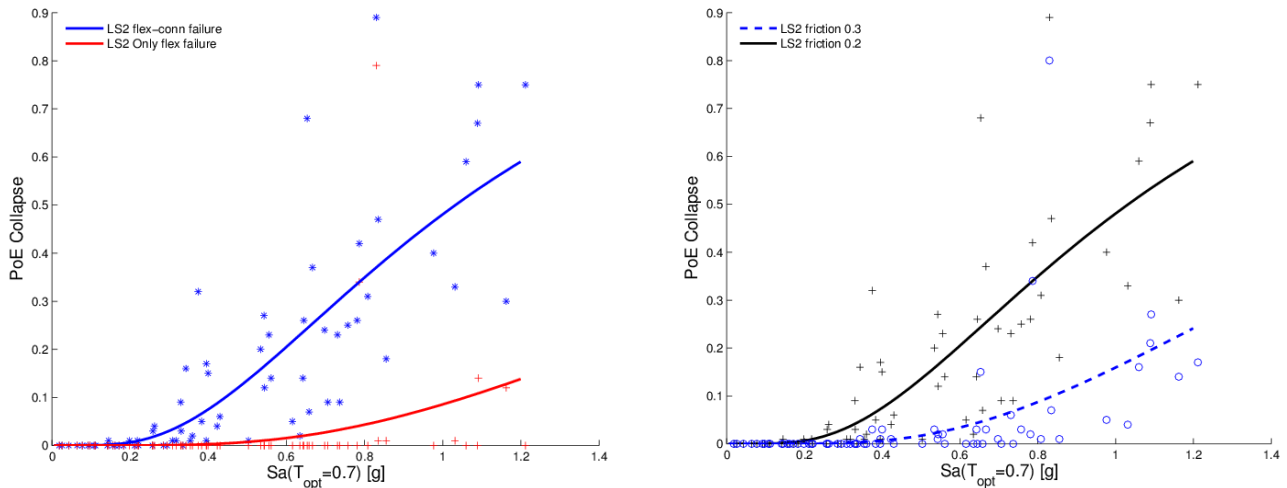


Fig. 11 Probability of exceedance derived for T1-CC. Collapse fragility curve considering or not the connection collapse, friction coefficient 0.2 (left), collapse fragility curve for two different friction coefficient (right)

connection and column failures, for a friction coefficient of 0.2. Fig. 11 on the right compares the combined collapse fragility curves obtained for the two different friction coefficients of 0.2 and 0.3. It is noticed that the connection failure is still predominant and as the figure on the right suggests, it is significantly affected by the value of the friction coefficient.

It is evident from Fig. 11 that the sensibility of the collapse fragility to the connection failure (i.e., to the connection friction coefficient) cannot be neglected and has to be addressed carefully. Despite the use of capacity design principles, also for the current-code designs, the influence of connection on the safety of the structure is still very high.

The reason can be found in the connection design procedure explained in section 5.2; the shear demand is used for the definition of number and size of steel bars, but the resistance of the connection is associated also with two other failure mechanisms, pry-out and concrete edge failure,

which depend only on geometry and materials and are not considered in the design process. The connection capacity is estimated as the sum of friction contribution and the smallest shear resistance (usually the concrete edge failure) associated with the three failure modes. Looking at Table 7 connection resistance of current-code designs is higher if compared with low-code designs, but not enough to avoid connection collapse in case of strong earthquake intensities.

8.2 Second modelling approach

The fragility curves obtained with the second modelling approach are presented for each independent mechanism (column and connection failure) and for the combined mechanism in Fig. 12 to Fig. 15. The model parameters (θ and σ) for the cumulative collapse fragility functions (considering both mechanisms) are reported in Table 9.

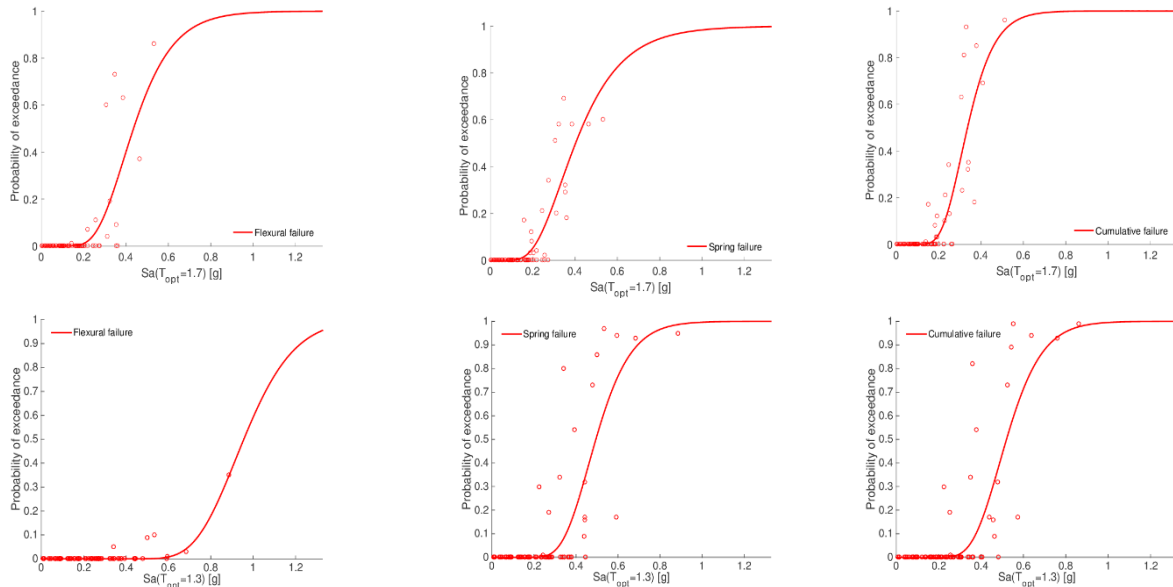


Fig. 12 Probability of exceedance derived for IC-T1-LC-4 (top) and IC-T1-LC-7 (bottom): collapse fragility curve considering only flexural collapse (left), only connection collapse (middle), both mechanisms (right)

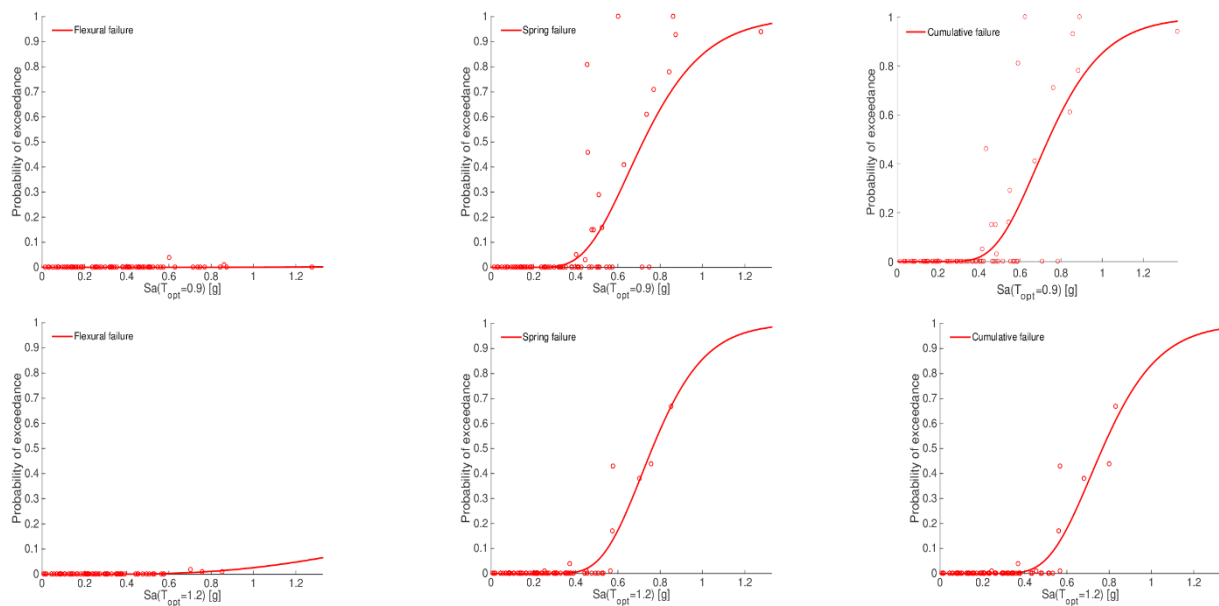


Fig. 13 Probability of exceedance derived for IC-T1-LC-10 (top) and IC-T1-CC (bottom): collapse fragility curve considering only flexural collapse (left), only connection collapse (middle), both mechanisms (right)

For the reasons explained before, the comparison between fragility curves obtained for different building classes is not valid; however, it is still possible to highlight some differences between code categories and building typologies.

It is observed in Figs. 12(top) and 14(top) that, for buildings in the low-code category, designed for 4% of the seismic weight, the fragilities corresponding to column collapse are comparable to those of connection failure. Conversely, for current-code designs (Figs. 13 and 15, bottom) and low-code buildings (Figs. 12 and 14, bottom; and Figs. 13 and 15, top), designed for high seismic intensities, the column fragility curves are negligible when

compared against the connection fragilities. This trend can be explained on the fact that columns of frames designed for high lateral forces, are able to resist demands equal or larger than the connection resistance.

On the contrary, in buildings designed for low horizontal forces, columns are more slender, and tend to collapse at forces below the connection capacity.

This second modelling approach reveals important differences not noticed in the first modelling approach, between building typologies 1 and 2 designed with the provisions of the low-code. As observed in Figs. 12 and 13(top), combined and individual collapse fragilities of the structural typology 1, increase in accordance with the

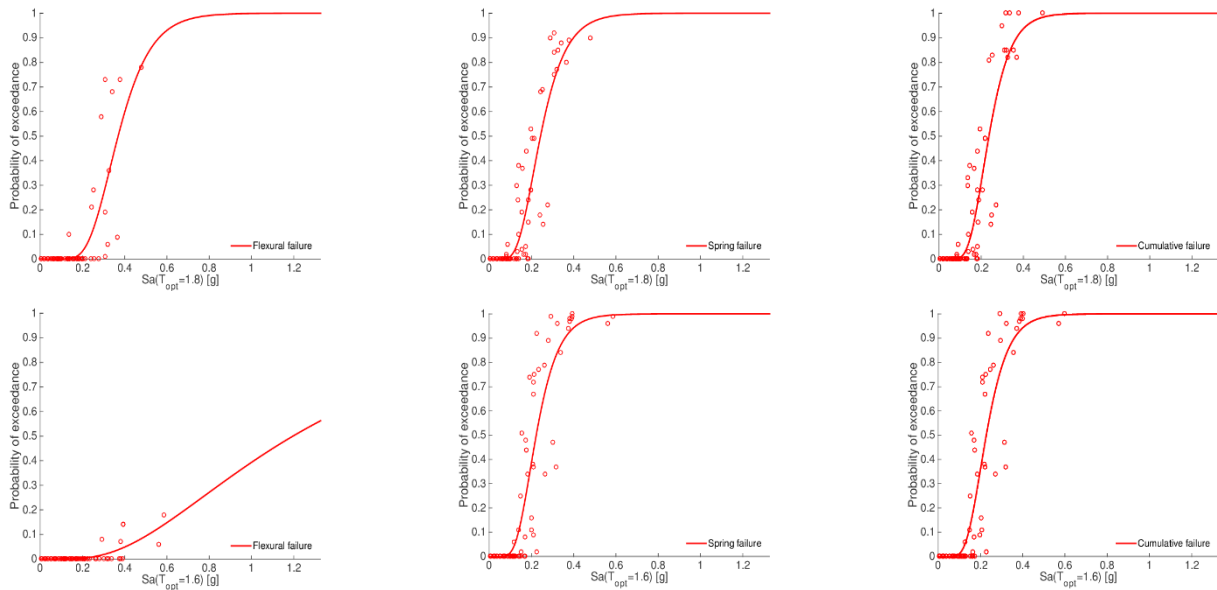


Fig. 14 Probability of exceedance derived for IC-T2-LC-4 (top) and IC-T2-LC-7 (bottom): collapse fragility curve considering only flexural collapse (left), only connection collapse (middle), both mechanisms (right)

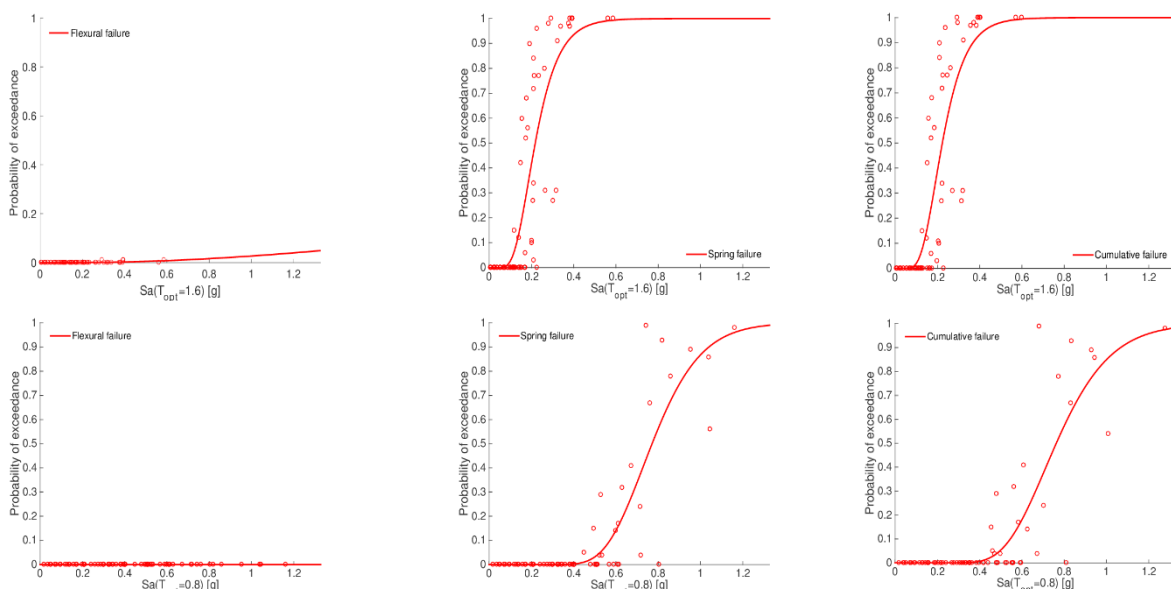


Fig. 15 Probability of exceedance derived for IC-T2-LC-10 (top) and IC-T2-CC (bottom): collapse fragility curve considering only flexural collapse (left), only connection collapse (middle), both mechanisms (right)

three lateral force levels (4%, 7% and 10% of the seismic weight) used in the design. Nonetheless, the counterparts in structural typology 2 (Figs. 14 and 15(top)) do not seem affected by the different seismic force levels applied in the design. Although it is recognised that the flexural failure probability decreases going from IC-T2-LC-4 to IC-T2-LC-10, the connections behaviour do not present any improvements and the probability of collapse is almost the same, independently from the seismic intensity used for the low-code design.

Comparing the fragility curves obtained for buildings designed according to the criteria of the low-code with the highest seismic intensity, against those for current code designs (Figs. 13 and 15), the latter presents a significant

reduction of probability of reaching collapse; the improvements produced by the last Italian building code are evident and higher spectral acceleration are required to reach collapse limit state; however, as seen in the first modelling approach, the connection collapse is still recurrent.

9. Conclusions

The aim of this study was to develop fragility functions for Italian RC precast industrial buildings, for further application in earthquake loss assessment. Given the lack of available literature on the fragility assessment of such

structures, against the good knowledge of the behaviour of regular cast-in-place buildings, special attention was given to the simplifications usually adopted in structural modelling. The design process was described with reference to three Italian building codes (two historic and the current code of record); with specific emphasis on the design of components that affect the response of the case study buildings (i.e., connection and column design). Particular attention was focused on the design and numerical modelling of beam-column connections, which are the principal cause of structural collapse, even for moderate earthquake intensities.

The frames were subjected to horizontal and vertical ground motions. Two modelling approaches for the beam-column connections were implemented in the numerical analysis. In the first approach, the connection was conceived as a hinge (pinned connection); and assessment of connection failure and beam collapse was obtained after post-processing of the results of the dynamic analyses. Results from this modelling approach showed that, in buildings designed for high lateral forces, the connection became the weak link, because they are not able to transmit the inertial forces to the columns. Furthermore, the results highlighted the sensibility of collapse fragilities to the friction coefficient adopted in the capacity model, and also the importance of considering the connection failure in the development of collapse fragilities.

The limitations of this modelling approach also provided justification for the consideration of a more explicit modelling technique. A second approach was developed in order to reproduce more realistically the behaviour of beam-column joints, of precast industrial buildings, subjected to seismic excitation. Two shear springs with limited ductility, and zero residual capacity, allow to simulate the resisting mechanisms of the connection (friction and steel dowel), their failure and the possible loss of support of the beam. Few past studies have adopted a similar modelling solution; but none of them has addressed the unseating of beams directly in the analysis. The capabilities of this modelling approach for the assessment of the collapse capacity and the derivation of collapse fragility curves for precast industrial buildings are evident.

As a general, the results demonstrate the efficiency of the current code provisions in reducing the collapse probability of contemporarily designed precast industrial buildings. On the other hand, the results obtained with the second modelling approach confirmed the conclusions found in the first approach: the connection is the most important component of the structure and largely controls the behaviour of the entire building. However, significant differences are noticed between the two approaches due to the different and more close-to-reality modelling solution of the second approach proposed in this paper.

It can be concluded that a set of fragility functions for Italian precast buildings is now available for earthquake loss assessment and can be employed for the development of seismic risk mitigation actions.

Acknowledgements

The authors would like to thank the Seismic Risk Prevention Area of Tuscany Region, who kindly shared their database regarding the geometrical properties of the industrial structures. The authors are very grateful for the valuable contribution of Davide Bolognini, whose expert advice on Italian precast structures is most appreciated. The authors are also very grateful to Manya Deyanova for discussions and input on the seismic behaviour of RC precast industrial buildings which helped improve the modelling approach used herein.

The authors would also like to acknowledge the European Commission, through its FP7 programme, for the financial support provided to the STREST research programme, under which this work has been partially funded.

Finally, the authors would also like to express their gratitude for the financial support provided by the Italian Department of Civil Protection (DPC-Dipartimento della Protezione Civile) through the financing of EUCENTRE-DPC (2014-2016) applied research programs, under the framework of which this work has been partially funded.

References

- Aquiar, E.A.B., Belluccio, E.K. and El Debs, M.K. (2011), "Behavior of grouted dowels used in precast concrete connections", *Struct. Concrete*, **13**(2), 84-94.
- Ahmad, N., Crowley, H. and Pinho, R. (2011), "Analytical fragility functions for reinforced concrete and masonry buildings and buildings aggregates of Euro-Mediterranean regions - UPAV methodology", Internal Report, Syner-G Project 2009/2012.
- Artioli, E., Battaglia, R. and Tralli, A. (2013), "Effects of May 2012 Emilia earthquake on industrial buildings of early '900 on the Po river line", *Eng. Struct.*, **56**, 1220-1233.
- Babic, A. and Dolsek, M. (2016), "Seismic fragility functions of industrial precast building classes", *Eng. Struct.*, **118**, 357-370.
- Banerjee, A.K., Pramanik, D. and Roy, R. (2016), "Seismic structural fragilities: Proposals for improved methodology per spectral matching of accelerogram", *Eng. Struct.*, **111**, 538-551.
- Belleri, A., Brunesi, E., Nascimbene, R., Pagani, M. and Riva, P. (2014), "Seismic performance of precast industrial facilities following major earthquakes in Italian territory", *J. Perform. Constr. Facil.*, **29**(5), 04014135.
- Belleri, A., Torquati, M., Riva, P. and Nascimbene, R. (2015), "Vulnerability assessment and retrofit solutions of precast industrial structures", *Earthq. Struct.*, **8**(3), 801-820.
- Bellotti, D., Casotto, C., Crowley, H., Deyanova, M.G., Fianchisti, G., Germagnoli, F., Lucarelli, E., Riva, S. and Nascimbene, R. (2014), "Capannoni monopiano prefabbricati: distribuzione probabilistica dei sistemi e sottosistemi strutturali dagli anni sessanta ad oggi", *Progettazione Sismica*, **5**(3), 41-70.
- Bolognini, D., Borzi, B. and Pinho, R. (2008), "Simplified Pushover-Based Vulnerability Analysis of Traditional Italian RC precast structures", *Proceedings of the 14th World Conference on Earthquake Engineering*, Beijing, China, October.
- Brunesi, E., Nascimbene, R., Bolognini, D. and Bellotti, D. (2015), "Experimental investigation of the cyclic response of reinforced precast concrete framed structures", *PCI J.*, **60**(2), 57-79.

- Calvi, G.M., Bolognini, D. and Nascimbene, R. (2006), "Seismic design of precast RC structures: state of the art and construction practise in the Italian context", *Proceedings of the 2nd fib Congress*, Naples, Italy, June.
- Calvi, G.M., Pinho, R., Magenes, G., Bommer, J.J., Restrepo-Vélez, L.F. and Crowley, H. (2006), "Development of seismic vulnerability assessment methodologies over the past 30 years", *ISET J. Earthq. Technol.*, **43**(3), 75-104.
- Calvi, G.M., Filippetto, M., Bolognini, D. and Nascimbene, R. (2007), "Seismic design and retrofit of traditional Italian RC precast structures", *Proceedings of the Thematic Conference on Computational Methods*, Crete, Greece, June.
- Casotto, C., Silva, V., Crowley, H., Nascimbene, R. and Pinho, R. (2015), "Seismic Fragility of Italian RC Precast Industrial Structures", *Eng. Struct.*, **94**, 122-136.
- Clementi, F., Scalbi, A. and Lenci, S. (2016), "Seismic performance of precast reinforced concrete buildings with dowel pin connections", *J. Build. Eng.*, **7**, 224-238.
- Crowley, H., Pinho, R. and Bommer, J.J. (2004), "A probabilistic displacement-based vulnerability assessment procedure for earthquake loss estimation", *Bull. Earth. Eng.*, **2**(2), 173-219.
- Decreto Ministeriale 3 marzo 1975 (1975), "Approvazione delle norme tecniche per le costruzioni in zone sismiche", (in Italian).
- Decreto Ministeriale 3 dicembre 1987 (1987), "Norme tecniche per la progettazione, esecuzione e collaudo delle costruzioni prefabbricate", (in Italian).
- Decreto Ministeriale 14 Febbraio 1992 (1992), "Norme tecniche per l'esecuzione delle opere in cemento armato normale e precompresso e per le strutture metalliche", (in Italian).
- Decreto Ministeriale 16 gennaio 1996 (1996), "Norme tecniche per le costruzioni in zone sismiche", (in Italian).
- Decreto Ministeriale 14 gennaio 2008 (2008), "Norme Tecniche per le Costruzioni", (in Italian).
- Deyanova, M., Pampanin, S. and Nascimbene, R. (2014), "Assessment of single-storey precast concrete industrial buildings with hinged beam-column connections with and without dowels", *Proceedings of the 2nd European conference on earthquake engineering and seismology*, Istanbul, Turkey.
- Ercolino, M., Magliulo, G. and Manfredi, G. (2016), "Failure of a precast RC building due to Emilia-Romagna earthquakes", *Eng. Struct.*, **118**, 262-273.
- European Organisation for Technical Approvals - EOTA, (2001), "ETAG 001 Guideline for European technical approval of metal anchors for use in concrete, Annex C: Design methods".
- European Organisation for Technical Approvals - EOTA, (2013), "Technical report design of metal anchors for use in concrete under seismic actions".
- Ferrini, M., Lucarelli, E., Baglione, M., Borsier, S., Bortone, G., Ginori, R., Mangone, F., Mannella, A., Martinelli, A., Milano, L., Ntibarikure, M.C., Pirisi, P., Spampanato, A. and Tucci, G. (2007), "DOCUP Toscana 2000-2006 - Azione 2.8.3: Riduzione del rischio sismico nelle aree produttive - Esiti dell'indagine di primo livello", *Proceedings of the 12th Conference of Seismic Engineering in Italy*, Pisa, Italy. (in Italian)
- Karantoni, T., Lyrantzaki, F., Tsionis, G. and Fardis, M.N. (2011), "Analytical fragility functions for masonry buildings and building aggregates - UPAT methodology", Internal Report, Syner-G Project.
- Kramer, S.L. (1996), "Geotechnical earthquake engineering", Prentice-Hall International Series in Civil Engineering.
- Iervolino, I., Chioccarelli, E. and Convertito, V. (2011), "Engineering design earthquakes from multimodal hazard disaggregation", *Soil Dyn. Earthq. Eng.*, **31**(9), 1212-1231.
- Magliulo, G., Capozzi, V., Fabbrocino, G. and Manfredi, G. (2011), "Neoprene-concrete friction relationships for seismic assessment of existing precast buildings", *Eng. Struct.*, **33**(2), 532-538.
- Magliulo, G., Ercolino, M., Cimmino, M., Capozzi, V. and Manfredi, G. (2014), "FEM analysis of the strength of RC beam-to-column dowel connections under monotonic actions", *Constr. Build. Mater.*, **69**, 271-284.
- Magliulo, G., Ercolino, M., Petrone, C., Coppola, O. and Manfredi, G. (2012), "The influence of connections on the seismic response exhibited by precast structures during Emilia earthquake", *Progettazione Sismica*, **3**, 121-130.
- Magliulo, G., Ercolino, M., Petrone, C., Coppola, O. and Manfredi, G. (2014b), "The Emilia earthquake: seismic performance of precast RC buildings", *Earthq. Spectra*, **30**(2), 891-912.
- Mander, J.B., Priestley, M.J.N. and Park, R. (1988), "Theoretical stress-strain model for confined concrete", *J. Struct. Eng.*, ASCE, **114**(8), 1804-1826.
- Marzo, A., Marghella, G. and Indirli, M. (2012), "The Emilia-Romagna earthquake: damages to precast/prestressed reinforced concrete factories", *Ingegneria Sismica*, **29**(2-3), 132-147.
- Matlab, <http://www.mathworks.com/> (2010), The MathWorks Inc.
- McKenna, F., Scott, M.H. and Fenves, G.L. (2010), "Nonlinear finite element analysis software architecture using object composition", *J. Comput. Civ. Eng.*, **24**(1), 97-105.
- McKenna, F. and Fenves, G.L. (2010), Open system for earthquake engineering simulation (OpenSees), Pacific Earthquake Engineering Research Center; <http://opensees.berkeley.edu/>.
- Menegotto, M., Pinto P.E. (1973), "Method of analysis for cyclically loaded R.C. plane frames including changes in geometry and non-elastic behaviour of elements under combined normal force and bending", *Symposium on the Resistance and Ultimate Deformability of Structures Acted on by Well Defined Repeated Loads*, International Association for Bridge and Structural Engineering, Zurich, Switzerland.
- Ordinanza del Presidente del Consiglio dei Ministri n. 3274 del 20 marzo 2003 (2003), "Primi elementi in materia di criteri generali per la classificazione sismica del territorio nazionale e di normative tecniche per le costruzioni in zona sismica". (in Italian)
- Ozmen, H.B., Inel, M., Meral, E. and Bucakli, M. (2010), "Vulnerability of low and mid-Rise reinforced concrete buildings in Turkey", *14th European Conference on Earthquake Engineering*, Ohrid, Macedonia, September.
- Polese, M., Verderame, G.M., Mariniello, C., Iervolino, I. and Manfredi, G. (2008), "Vulnerability analysis for gravity load designed RC buildings in Naples - Italy", *J. Earthq. Eng.*, **12**(S2), 234-245.
- Psycharis, L.N. and Mouzakis, H.P. (2012), "Shear resistance of pinned connections of precast members to monotonic and cyclic loading", *Eng. Struct.*, **41**, 413-327.
- Savoia, M., Mazzotti, C., Buratti, N., Ferracuti, B., Bovo, M., Ligabue, V. and Vincenzi, L. (2012), "Damage and collapses in industrial precast buildings after the Emilia earthquake", *Ingegneria Sismica*, **29**(2-3), 120-131.
- Scott, B.D., Park, R. and Priestley, M.J.N. (1982), "Stress-strain behavior of concrete confined by overlapping hoops at low and high strain rates", *ACI J. Proc.*, **79**(3), 13-27.
- Seissoft - SeismoStruct (2016), "A computer program for static and dynamic nonlinear analysis of framed structures", available from URL: www.seissoft.com.
- Senel, M.S. and Kayhan, A.H. (2010), "Fragility based damage assessment in existing precast industrial buildings: A case study for Turkey", *Struct. Eng. Mech.*, **34**(1), 39-60.
- Silva, V., Crowley, H., Varum, H. and Pinho, R. (2015), "Investigation of the characteristics of Portuguese regular moment-frame RC buildings and development of a vulnerability model", *Bull. Earthq. Eng.*, **13**(5), 1455-1490.

- Toniolo, G. (2012), "SAFECAST Project: European research on seismic behavior of the connection of precast structures", *Proceedings of the 15th World conference on earthquake engineering*, Lisbon, Portugal, September.
- Verderame, G.M., Stella, A. and Cosenza, E. (2001), "Mechanical properties of reinforcing steel adopted in R.C. structures in the age '60", *Proceedings of the 10th National ANIDIS Conference: Seismic Engineering in Italy*, Potenza-Matera, Italy, September. (in Italian)
- Watson-Lamprey, J. and Abrahamson, N. (2006), "Selection of ground motion time series and limits on scaling", *Soil Dyn. Earthq. Eng.*, **26**(5), 477-482.
- Yazgan, U. (2015), "Empirical seismic fragility assessment with explicit modeling of spatial ground motion variability", *Eng. Struct.*, **100**, 479-489.
- Zoubek, B., Fischinger, M. and Isaković, T. (2014) "Seismic response of dowel connections in precast industrial buildings", *Proceedings of the 2nd European conference on earthquake engineering and seismology*, Istanbul, Turkey, August.
- Zoubek, B., Fischinger, M. and Isaković, T. (2015), "Estimation of the cyclic capacity of beam-to-column dowel connections in precast industrial buildings", *Bull. Earthq. Eng.*, **13**(7), 2145-2168.